



HAL
open science

Multiple Camera Tracking of Rigid Objects

Frederick Martin, Radu Horaud

► **To cite this version:**

Frederick Martin, Radu Horaud. Multiple Camera Tracking of Rigid Objects. The International Journal of Robotics Research, 2002, 21 (2), pp.97–113. 10.1177/027836402760475324 . inria-00590160

HAL Id: inria-00590160

<https://inria.hal.science/inria-00590160>

Submitted on 3 May 2011

HAL is a multi-disciplinary open access archive for the deposit and dissemination of scientific research documents, whether they are published or not. The documents may come from teaching and research institutions in France or abroad, or from public or private research centers.

L'archive ouverte pluridisciplinaire **HAL**, est destinée au dépôt et à la diffusion de documents scientifiques de niveau recherche, publiés ou non, émanant des établissements d'enseignement et de recherche français ou étrangers, des laboratoires publics ou privés.

Multiple-camera Tracking of Rigid Objects*

Frédéric Martin and Radu Horaud
INRIA Rhône-Alpes & GRAVIR-CNRS
655, avenue de l'Europe
38330 Montbonnot Saint-Martin, FRANCE

International Journal of Robotics Research, vol. 21, no. 2, pages 97–113,
February 2002

Abstract

In this paper we describe a method for tracking rigid objects using one or several cameras. The tracking process consists of aligning a 3-D model representation of an object with image contours by measuring and minimizing the image error between predicted model points and image contours. The tracker behaves like a visual servo loop where the internal and external camera parameters are updated at each new image acquisition. We study in detail the Jacobian matrix associated with this minimization process in the presence of both point-to-point and point-to-contour matches. We establish the minimal number of matches that are needed as well as the singular configurations leading to a rank-deficient Jacobian matrix. We find a mathematical link between the point-to-point and point-to-contour cases. Based on this link we show that the latter has the same kind of singularities than the former. Moreover, we study multiple camera configurations which optimize the robustness of the method in the presence of single-camera singularities, bad, noisy, or missing data. Extensive experiments done with a complex ship part and with up to three cameras validate the method. In particular we show that the tracker may well be used as a camera calibration procedure.

*This work was sponsored by the European Commission through Esprit-IV Reactive LTR project number 26247 VIGOR (Visually Guided Robots Using Uncalibrated Cameras), <http://www.inrialpes.fr/VIGOR/>.

1 Introduction, background, and approach

The problem of localizing and tracking moving objects using one or several cameras has been an active research topic. Objects fall into several categories, from rigid, deformable, articulated and rigid, to articulated and deformable. A common approach consists of using an object model and of estimating the position and orientation of this model such that some image-based error is minimized. The image error describes the discrepancy between measured object features and predicted model features. The ability to properly move the model such that it optimally corresponds to the actual object depends on a number of factors. Roughly speaking, the 3-D parameters associated with the object’s behaviour (motion parameters, shape deformation parameters, joint parameters for an articulated object, etc.) are related to the image error by a Jacobian matrix.

With only one camera there are inherent ambiguities and singularities. Indeed, one image configuration may lead to a number of 3-D actions and Jacobian singularities may lead to no action at all. Therefore, it may be advantageous to use several cameras instead of one. From a practical point of view this raises the problem of dealing with multiple camera geometry. It is more tedious to calibrate a multiple-camera system and to update the calibration data than to calibrate a single camera. Moreover, the vast majority of previous approaches consider the multi-camera system as a stereo device requiring that each object feature is viewed in at least two images and that image-to-image feature matches are provided.

In this paper we propose a multi-camera based method for tracking rigid objects. A geometric model of the tracked object is provided in advance. The method consists of a “visual servoing” approach applied to the object model, [12]: At each iteration of the tracking process the image error between model and object features allows to update the parameters associated with the position and orientation of the model.

First, we investigate the case of one camera. We establish the link between point-to-point tracking and point-to-contour tracking. We analyse both the cases of fixed and varying camera internal parameters. We study the singularities of the Jacobian matrix and we reveal the cases where single-camera tracking cannot be properly performed.

Second, we investigate the case of several cameras. We show how the single-camera case can be used to calibrate the multiple-camera layout. We establish the tracking formulation which allows a rigid camera layout with possibly varying internal camera parameters. This formulation consists of running in parallel several single-camera trackers and does not require any

image-to-image correspondences. We show how most of the single-camera singularities can be avoided by using two or more cameras.

Third, we describe an implementation using three cameras and a complex rigid object. Each camera observes a different object part and therefore the system is very robust with respect to partial occlusions simultaneously occurring in several images and with respect to total occlusion of one or two cameras.

1.1 Previous work

The idea of using pose for tracking stems from the work of Lowe [16] who used line-segment matches and the Levenberg-Marquardt non-linear minimization method. Tracking with variable internal camera parameters has been introduced by Kinoshita and Deguchi [13] who perform visual servoing and camera calibration *simultaneously*. Espiau performed an in-depth analysis of the convergence of visual servoing in the presence of varying focal length [7].

Harris [9] and Armstrong and Zisserman [1] proposed to predict a model contour in the image and to search around this prediction for image points that are likely to lie on a matching contour. They apply this technique to the case of straight lines and use a robust method to fit a line to the image points. Drummond and Cipolla [5, 3, 6] showed that it is possible to cast the rigid model tracking problem into a linear problem using the Lie algebra of the rigid motion - the kinematic screw. They suggest a series of papers dealing with a complex 3-D object (a ship part) and with articulated objects. The approach of Drummond and Cipolla is interesting because it relies only weakly on point or line matches. Instead their technique relies on contour-to-points matching. They show that their approach can be used for calibrating a camera. Other similar approaches to tracking using an image prediction and searching in a window around this prediction can be found in [21] and [24].

All these approaches to tracking consider only one camera and put emphasis on the data association problem. Multi-view tracking has been barely investigated. There are several ways of using several cameras. One way is to consider the multi-camera setup as a 3-D sensor, capture 3-D measurements, and perform the tracking directly in 3-D space, [23], [2]. Another way is to use the epipolar constraint into the tracking loop itself and Lamirov et al. [15] combine the tracking equations with the epipolar geometry constraint. Finally, when the cameras are far apart, there are very few image-to-image correspondences and single camera trackers may be performed in

parallel. Thompson et al. [22] extended the work of Harris and of Armstrong and Zisserman to multiple cameras and parallel trackers. They studied the improvements in performance using several cameras rather than using one camera. They describe an interesting and original teleoperation application where synthetic views are produced on-line thus maintaining, at a distance, visual information about the spatial distribution and location of polyhedral objects.

In this paper we derive an explicit algebraic expression for the Jacobian matrix associated with point-to-contour correspondences. Although in the past robust results were obtained with this type of data association, none thoroughly studied the algebraic structure of the Jacobian, the minimal data sets necessary to run a tracker, and the possibly singular configurations which lead to tracking failures. Based on this analysis we are able to show that a multiple-camera approach based on point-to-contour correspondences lead to a robust rigid-object tracker that can deal with large occlusions.

Previous work on object tracking has mainly dealt with off-line calibrated cameras (with the notable exception of [6]). This means that on-line changes (focus setting, zooming, etc.) cannot be taken into account and they are likely to affect the accuracy of inter-camera calibration and of the pose parameters. The possibility to adjust these parameters during tracking is thoroughly investigated and evaluated in this paper.

1.2 Paper organization

The remaining of this paper is organized as follows. Section 2 reviews the problem of tracking a rigid object using a perspective camera model. The relationship between the pose parameters (to be estimated by the tracker) and errors associated with the internal camera parameters is thoroughly investigated. Rigid object tracking is treated as a minimization problem and explicit formulae are derived for two types of image-to-model matches: point-to-point and point-to-contour assignments. Section 3 analyses the singularities associated with point-to-point assignments while section 4 provides a similar analysis for point-to-contour assignments. In particular, singular cases are revealed especially when the internal camera parameters are allowed to vary. Multiple-camera tracking is studied in section 5 where it is shown that the singularities associated with one camera disappear when two or more cameras are being used. Finally section 6 describes extensive experiments that illustrate all the variations of the tracking method.

2 Problem formulation

Mathematical notations. The following notations will be used throughout the paper. Bold characters represent matrices, italic bold characters represent vectors and roman characters represent scalars.

Without loss of generality we consider a moving rigid object observed by one camera. Tracking consists of a model being moved such that its apparent position and orientation with respect to the camera corresponds to the real position and orientation of the object. Let $\mathbf{s}_0 = (\mathbf{m}_1^0, \dots, \mathbf{m}_k^0)$ be a set of model points projected onto the image based on the current prediction, and let \mathbf{s} be the set of corresponding image points. The relationship between the model velocity and its apparent image velocity is:

$$\dot{\mathbf{s}} = \mathbf{J}\mathbf{T}$$

where \mathbf{T} is the kinematic screw associated with the 3D model motion. The error between the predicted model position and the actual object position may be measured from their image projections:

$$\mathbf{e} = \mathbf{C}(\mathbf{s}_0 - \mathbf{s})$$

Where \mathbf{C} is combination matrix allowing to consider more measurements than the number of degrees of freedom (six in this case – three for the rotational velocity vector and three for the translational velocity vector). A common choice which insures convergence is to set $\mathbf{C} = \mathbf{J}^\top$.

The objective is to move the model such that the image error decreases:

$$\lambda \mathbf{J}^\top (\mathbf{s}_0 - \mathbf{s}) = -\mathbf{J}^\top \dot{\mathbf{s}} = -\mathbf{J}^\top \mathbf{J}\mathbf{T}$$

which allows as solution:

$$\mathbf{T} = \lambda (\mathbf{J}^\top \mathbf{J})^{-1} \mathbf{J}^\top (\mathbf{s} - \mathbf{s}_0) \quad (1)$$

This is the basic visual servoing equation which is solved in order to maintain $\mathbf{s} - \mathbf{s}^*$ as small as possible. In order to apply this formulation to the tracking problem, one may approximate the velocity screw by:

$$\mathbf{T} = \frac{d\mathbf{x}}{dt} = \frac{\mathbf{x} - \mathbf{x}_0}{t - t_0}$$

Hence, the equation above allows the incremental update of the pose parameters \mathbf{x} :

$$\mathbf{x} = \mathbf{x}_0 + \lambda(t - t_0) (\mathbf{J}^\top \mathbf{J})^{-1} \mathbf{J}^\top (\mathbf{s} - \mathbf{s}_0) \quad (2)$$

2.1 Camera model

The model-based object tracking just described assumes a pinhole camera model, i.e., an object point projects onto an image point using the well known camera projection matrix:

$$\tilde{\mathbf{m}} = \mathbf{K} \begin{bmatrix} \mathbf{R} & \mathbf{t} \end{bmatrix} \tilde{\mathbf{M}} \quad (3)$$

where $\tilde{\mathbf{m}}$ is a homogeneous 3-vector describing the projective coordinates of an image point, \mathbf{K} is the matrix of internal camera parameters, \mathbf{R} is a rotation matrix, \mathbf{t} is a translation vector, and $\tilde{\mathbf{M}}$ is a homogeneous 4-vector describing the coordinates of a model point.

The internal camera parameters are f (horizontal and vertical scale factor, or focal length) and u_0 and v_0 (image coordinates of optical center):

$$\mathbf{K} = \begin{bmatrix} f & 0 & u_0 \\ 0 & f & v_0 \\ 0 & 0 & 1 \end{bmatrix}$$

This is a simplified camera model since it is well known that the horizontal to vertical scale factor can be estimated off-line, once for ever, and the value thus estimated is stable over time and over changes in camera settings.

2.2 The image Jacobian

The 2-vector \mathbf{m} describes the pixel coordinates associated with the projection $\tilde{\mathbf{m}}$. By taking the time derivatives we obtain the classical relationship:

$$\frac{d\mathbf{m}}{dt} = \mathbf{J}_m \begin{pmatrix} v_x \\ v_y \\ v_z \\ w_x \\ w_y \\ w_z \\ \frac{df}{dt} \\ \frac{du_0}{dt} \\ \frac{dv_0}{dt} \end{pmatrix} \quad (4)$$

with the kinematic screw $\mathbf{T}^\top = (v_x \ v_y \ v_z \ w_x \ w_y \ w_z)$ and with:

$$\mathbf{J}_m = f \begin{bmatrix} -\frac{1}{z} & 0 & \frac{x}{z^2} & \frac{xy}{z^2} & -\left(1 + \frac{x^2}{z^2}\right) & \frac{y}{z} & \frac{x}{zf} & \frac{1}{f} & 0 \\ 0 & -\frac{1}{z} & \frac{y}{z^2} & \left(1 + \frac{y^2}{z^2}\right) & -\frac{xy}{z^2} & \frac{-x}{z} & \frac{y}{zf} & 0 & \frac{1}{f} \end{bmatrix} \quad (5)$$

where $(x \ y \ z)$ are the Euclidean coordinates of point M expressed in camera frame.

2.3 Camera model errors

The camera parameters may be unknown, partially known, or badly known. One important feature of the tracking algorithm described below is that it can accommodate with rough estimates of these parameters which are updated during tracking.

We analyse the effect of badly known camera parameters onto the pose parameters. Let \mathbf{K} be the exact camera parameters and let \mathbf{R} and \mathbf{t} be the pose parameters associated with \mathbf{K} and with the point correspondences $\mathbf{m} \leftrightarrow \mathbf{M}$. Let $\hat{\mathbf{K}}$ be an estimation of the true camera parameters. With these estimated parameters one can associate estimated pose parameters $\hat{\mathbf{R}}$ and $\hat{\mathbf{t}}$. The projection equation holds in both these cases:

$$\tilde{\mathbf{m}} = \hat{\mathbf{K}} \begin{bmatrix} \hat{\mathbf{R}} & \hat{\mathbf{t}} \end{bmatrix} \tilde{\mathbf{M}} = \mathbf{K} \begin{bmatrix} \mathbf{R} & \mathbf{t} \end{bmatrix} \tilde{\mathbf{M}}$$

We have:

$$\tilde{\mathbf{m}} = \mathbf{K} \begin{bmatrix} \mathbf{K}^{-1}\hat{\mathbf{K}}\hat{\mathbf{R}} & \mathbf{K}^{-1}\hat{\mathbf{K}}\hat{\mathbf{t}} \end{bmatrix} \tilde{\mathbf{M}}$$

By writing $\hat{\mathbf{K}} = \mathbf{K} + d\mathbf{K}$ and by first-order Taylor expansion we obtain, [11]

$$\mathbf{K}'^{-1}\mathbf{K} = \mathbf{I} - \begin{bmatrix} \frac{df}{f} & 0 & \frac{du_0}{f} \\ 0 & \frac{df}{f} & \frac{dv_0}{f} \\ 0 & 0 & 0 \end{bmatrix} = \mathbf{I} + \mathbf{K}_\epsilon \quad (6)$$

The pose parameters are affected by these internal parameter errors as follows:

$$\begin{aligned} \hat{\mathbf{R}} &= \mathbf{R} - \mathbf{K}_\epsilon \mathbf{R} \\ \hat{\mathbf{t}} &= \mathbf{t} - \mathbf{K}_\epsilon \mathbf{t} \end{aligned}$$

The estimation of f , u_0 and v_0 is affected by the value of f . For small focal lengths the internal parameters have equal importance. For large focal lengths, the accuracy of f is intrinsically more crucial than the accuracy of the optical center. If the focal center lies at approximately the image center, the value of f is, on an average, 4-5 times greater than the values of u_0 and v_0 . Therefore, the ability to track in the presence of variable focal length, estimate and correct its value on line is an important feature.

2.4 Tracking as a minimization problem

We consider now a more general tracking problem where the object is observed simultaneously by several cameras with possibly varying internal camera parameters. Let \mathbf{q} denote the state-vector associated with such a setup:

this vector encapsulates the pose parameters of the object with respect to a global camera centered frame as well as the internal parameters associated with the camera models. Therefore, the model predictions \mathbf{s}_0 are a function of \mathbf{q} .

One must distinguish between two cases:

1. Tracking based on point-to-point correspondences
2. Tracking based on point-to-contour correspondences

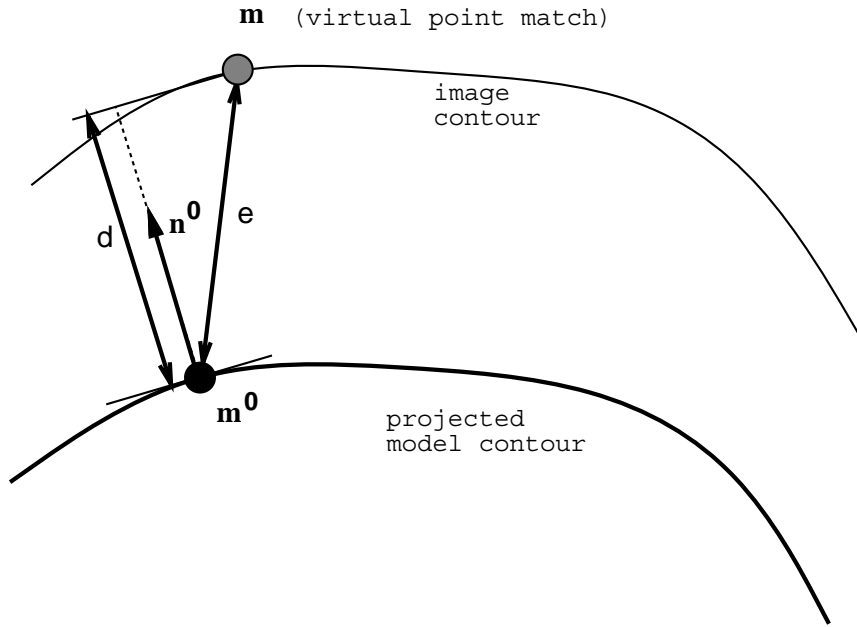


Figure 1: A model contour is predicted in the image and a point location \mathbf{m}^0 along this contour is considered. For point-to-point correspondences, it is sufficient to search for a matching point \mathbf{m} end to determine the distance e between these points. For point-to-contour correspondences the strategy consists of raising a normal to the model contour at location \mathbf{m}^0 , finding the intersection of the line supporting the normal vector with the matching image contour, and determining the distance from \mathbf{m}^0 to the image contour. The algebraic expression of this true point-to-contour distance can be approximated by $d = \mathbf{n}^0 \cdot (\mathbf{m} - \mathbf{m}^0)$.

These two cases are illustrated on Figure 1. In the first case (point-to-point) the function to be minimized may be written as the sum of the Euclidean distances from the predicted model point \mathbf{m}_i^0 to its image match

\mathbf{m}_i :

$$Q_1(\mathbf{q}) = \frac{1}{2} \sum_{i=1}^n \|\mathbf{m}_i^0(\mathbf{q}) - \mathbf{m}_i\|^2 = \frac{1}{2} \|\mathbf{s} - \mathbf{s}_0\|^2$$

Therefore, the general form of the minimization problem is, in this case:

$$Q_1(\mathbf{q}) = \frac{1}{2} \mathbf{r}(\mathbf{q})^\top \mathbf{r}(\mathbf{q}) \quad (7)$$

with:

$$\mathbf{r} = \mathbf{s} - \mathbf{s}_0$$

In practice it is well known that it is difficult to obtain point-to-point correspondences. A current approach is to project a model contour onto the image using the current pose and camera parameters, search in a direction normal to the predicted model contour, find a corresponding image point lying onto a contour, and measure the distance to this point [19], [4]. For a projected model point \mathbf{m}_i^0 and a normal direction \mathbf{n}_i^0 , this distance is approximated by, e.g., Figure 1:

$$d_i(\mathbf{q}) = \mathbf{n}_i^0(\mathbf{q}) \cdot (\mathbf{m}_i^0(\mathbf{q}) - \mathbf{m}_i)$$

Notice that this formula is exact for straight-line contours and hold only approximatively for curved contours. The function to be minimized may be written as:

$$Q_2(\mathbf{q}) = \frac{1}{2} (\mathbf{N}(\mathbf{q})\mathbf{r}(\mathbf{q}))^\top \mathbf{N}(\mathbf{q})\mathbf{r}(\mathbf{q}) = \frac{1}{2} \sum_{i=1}^n d_i^2 \quad (8)$$

Matrix \mathbf{N} of size $n \times 2n$ contains the normals to the projected model contours. Its rank is equal to n :

$$\mathbf{N} = \begin{bmatrix} n_{1u} & n_{1v} & 0 & 0 & \dots & 0 & 0 \\ 0 & 0 & n_{2u} & n_{2v} & \dots & 0 & 0 \\ \vdots & & & & & & \\ 0 & 0 & 0 & 0 & \dots & n_{nu} & n_{nv} \end{bmatrix} \quad (9)$$

The first- (Jacobian) and second-order (Hessian) derivatives of Q_1 with respect to \mathbf{q} are:

$$\begin{aligned} \frac{dQ_1}{d\mathbf{q}} &= \mathbf{J}_1^\top(\mathbf{q})\mathbf{r}(\mathbf{q}) \\ \frac{d^2Q_1}{d\mathbf{q}^2} &= \mathbf{J}_1^\top(\mathbf{q})\mathbf{J}_1(\mathbf{q}) + \frac{d^2\mathbf{r}}{d\mathbf{q}^2}\mathbf{r}(\mathbf{q}) \end{aligned}$$

Where the Jacobian is defined by:

$$\mathbf{J}_1 = \frac{d\mathbf{r}(\mathbf{q})}{d\mathbf{q}}$$

We derive now the Jacobian matrix for point-to-contour correspondences:

$$\begin{aligned} \mathbf{J}_2 &= \frac{d(\mathbf{N}(\mathbf{q})\mathbf{r}(\mathbf{q}))}{d\mathbf{q}} \\ &= \mathbf{N}(\mathbf{q})\mathbf{J}_1 + \left(\sum_{i=1}^{i=k} \frac{\partial \mathbf{N}(\mathbf{q})}{\partial q_i} \right) \mathbf{r}(\mathbf{q}) \end{aligned}$$

Matrix \mathbf{N} contains the normals to the contour. Its derivatives may therefore be considered as second-order terms and therefore they can be neglected in the expression of the Jacobian. The latter becomes:

$$\mathbf{J}_2 = \mathbf{N}(\mathbf{q})\mathbf{J}_1(\mathbf{q}) \quad (10)$$

The rank of \mathbf{J}_2 is related to the rank of \mathbf{J}_1 by the formula:

$$r(\mathbf{J}_2) \leq \min(\text{rank}(\mathbf{J}_1), \text{rank}(\mathbf{N})) = \min(\text{rank}(\mathbf{J}_1), n) \quad (11)$$

because the rank of \mathbf{N} is equal to n . This will be useful for analysing the convergence of tracking.

A common way to solve this problem is to consider the Gauss-Newton approximation of the Hessian, $\frac{d^2Q}{d\mathbf{q}^2} = \mathbf{J}^\top(\mathbf{q})\mathbf{J}(\mathbf{q})$ and to perform a number of quadratic iterations. One such quadratic iteration writes for \mathbf{J}_1 (where there is a similar expression for \mathbf{J}_2):

$$\mathbf{q}^\diamond = \mathbf{q} - (\mathbf{J}_1^\top(\mathbf{q})\mathbf{J}_1(\mathbf{q}))^{-1} \mathbf{J}_1^\top(\mathbf{q})\mathbf{r}(\mathbf{q}) \quad (12)$$

In practice and due to time constraints, only one iteration is performed each time a new image is grabbed. Therefore, there are two situations:

- The object is static with respect to the camera in which case the method behaves like a non-linear pose estimation technique or
- The object moves in which case the method acts like an object tracker maintaining a pose estimation as close as possible to a previously computed solution.

Notice that the Gauss-Newton iteration given by eq. (12) is strictly equivalent to eq. (2). Both these equations require the Jacobian matrix to be of rank equal to the dimension of the state vector \mathbf{q} . In the sequel we analyse cases for which the Jacobian matrix has singularities. An alternative way to avoid such singularities is to consider trust-region minimization methods for solving eq. (7) or eq. (8), [16, 17], [20].

3 Point-to-point correspondences

The relationship between image measurements and incremental rigid motions allowing the model-to-object alignment is encapsulated in the Jacobian matrices \mathbf{J}_1 and \mathbf{J}_2 mentioned above. We distinguish the following cases:

1. Fixed internal camera parameters
2. Varying focal length
3. Varying internal camera parameters (focal length and optical center)

In the case of point-to-point correspondences, the Jacobian is of dimensions $2n \times k$ where n is the number of point correspondences and k is the number of parameters to be recovered (the dimension of \mathbf{q}). For the general case (varying internal parameters) and for one point-to-point match it has the algebraic structure given by eq. (5).

In the case of point-to-contour correspondences, the Jacobian is of dimension $n \times k$ where n is the number of point-to-contour correspondences.

In order to study potential failures of the tracking method and, possibly, avoid them we must analyse the rank of the Jacobian for the minimum number of points and contours, and determine geometric configurations for which the Jacobian is rank deficient.

3.1 Fixed internal camera parameters

There are six parameters to be estimated in this case (three for rotation and three for translation) and hence the least number of correspondences is equal to 3. This case was thoroughly studied within the convergence analysis of visual servoing methods. The Jacobian is rank deficient when (i) the image points are collinear or when (ii) the three model points together with the optical center lie on a cylinder:

$$\mathbf{J}_1 = \begin{bmatrix} \vdots & & & & & & \\ -\frac{1}{z_i} & 0 & \frac{x_i}{z_i^2} & \frac{x_i y_i}{z_i^2} & -\left(1 + \frac{x_i^2}{z_i^2}\right) & \frac{y_i}{z_i} & \\ 0 & -\frac{1}{z_i} & \frac{y_i}{z_i^2} & \left(1 + \frac{y_i^2}{z_i^2}\right) & -\frac{x_i y_i}{z_i^2} & \frac{-x_i}{z_i} & \\ \vdots & & & & & & \end{bmatrix} \quad (13)$$

3.2 Varying focal length

In this case there are seven parameters to be estimated. Therefore, a minimum of four correspondences are required. Due to the structure of the Jacobian matrix, a planar configuration with four (or more) points lying in a plane parallel to the image plane gives rise to a Jacobian of rank equal to 6. Indeed, for such a configuration, the depth parameters z_i are the same for all the points and the third column is proportional to the last column in the Jacobian matrix:

$$\mathbf{J}_1 = f \begin{bmatrix} \vdots \\ -\frac{1}{z_i} & 0 & \frac{x_i}{z_i^2} & \frac{x_i y_i}{z_i^2} & -\left(1 + \frac{x_i^2}{z_i^2}\right) & \frac{y_i}{z_i} & \frac{x_i}{z_i f} \\ 0 & -\frac{1}{z_i} & \frac{y_i}{z_i^2} & \left(1 + \frac{y_i^2}{z_i^2}\right) & -\frac{x_i y_i}{z_i^2} & \frac{-x_i}{z_i} & \frac{y_i}{z_i f} \\ \vdots \end{bmatrix} \quad (14)$$

This means that it is not possible to simultaneously track a planar object and estimated the focal length when this object lies in a plane parallel (or almost parallel) to the image plane. This singularity extends to the case where an arbitrary 3-D object is at a distance from the camera such the weak-perspective approximation becomes valid. In fact this configuration is the only known situation which does not allow the distinguish between variations in depth and variations in focal length.

3.3 Varying internal camera parameters

In this case there are 9 parameters to be estimated (provided that the camera's horizontal-to-vertical scale ratio is known) and hence the Jacobian must be of rank at least equal to 9. Again, a fronto-parallel planar object gives rise to a rank-deficient Jacobian matrix for the same algebraic reasons as above.

$$\mathbf{J}_1 = f \begin{bmatrix} \vdots \\ -\frac{1}{z_i} & 0 & \frac{x_i}{z_i^2} & \frac{x_i y_i}{z_i^2} & -\left(1 + \frac{x_i^2}{z_i^2}\right) & \frac{y_i}{z_i} & \frac{x_i}{z_i f} & \frac{1}{f} & 0 \\ 0 & -\frac{1}{z_i} & \frac{y_i}{z_i^2} & \left(1 + \frac{y_i^2}{z_i^2}\right) & -\frac{x_i y_i}{z_i^2} & \frac{-x_i}{z_i} & \frac{y_i}{z_i f} & 0 & \frac{1}{f} \\ \vdots \end{bmatrix} \quad (15)$$

4 Point-to-contour correspondences

The relationship between \mathbf{J}_2 and \mathbf{J}_1 established in the previous section – $\mathbf{J}_2 = \mathbf{N}\mathbf{J}_1$ – allows analysis of the singularities associated with this type

of correspondences. Unlike the point-to-point case, each point-to-contour match contributes with one row in the Jacobian matrix \mathbf{J}_2 . Therefore, twice more point-to-contour than point-to-point correspondences are necessary. At first glance this may appear as a disadvantage. In practice, it is easier to establish point-to-contour correspondences and hence a method based on such correspondences is likely to be more robust. It is often the case that several points match a single contour. It will be shown that in the case of linear contours, the minimum number of image lines required by the point-to-contour tracker is equal to the number of image points required by the point-to-point tracker.

In order to implement a tracker based on point-to-contour correspondences, the rank of the Jacobian matrix \mathbf{J}_2 must be equal to 9 (position, orientation, and varying internal camera parameters), 7 (position, orientation, and varying focal length), or to 6 (position and orientation). Consequently a minimum of 9, 7, or 6 matches are necessary. We analyse these situations in reverse order.

4.1 Fixed internal camera parameters

Without loss of generality we consider a set of colinear model points, i.e., model points lying on linear edges. Let A and B be two points belonging to a linear edge with camera coordinates $\mathbf{A} = (x_A \ y_A \ z_A)^\top$ and $\mathbf{B} = (x_B \ y_B \ z_B)^\top$. A third point M has as coordinates $\mathbf{M} = \mathbf{A} + \lambda(\mathbf{B} - \mathbf{A})$ or:

$$\begin{aligned} x_M &= x_A + \lambda(x_B - x_A) \\ y_M &= y_A + \lambda(y_B - y_A) \\ z_M &= z_A + \lambda(z_B - z_A) \end{aligned}$$

where λ is a free parameter, e.g., Figure 2.

These three model points project onto the image producing an image line and let $\mathbf{n} = (n_u \ n_v)^\top$ be the normal to this line. The pixel coordinates of \mathbf{n} can be computed from the coordinates of vectors \mathbf{A} and \mathbf{B} [20]:

$$\mathbf{n} = \frac{\mathbf{p}}{\|\mathbf{p}\|} \text{ with } \mathbf{p} = \begin{pmatrix} p_u \\ p_v \end{pmatrix} = \begin{pmatrix} y_B z_A - y_A z_B \\ x_A z_B - x_B z_A \end{pmatrix}$$

Matrix \mathbf{N} , containing the image normals to the predicted model contour, has a simple expression for three collinear points:

$$\mathbf{N} = \frac{1}{\|\mathbf{p}\|} \begin{bmatrix} p_u & p_v & 0 & 0 & 0 & 0 \\ 0 & 0 & p_u & p_v & 0 & 0 \\ 0 & 0 & 0 & 0 & p_u & p_v \end{bmatrix}$$

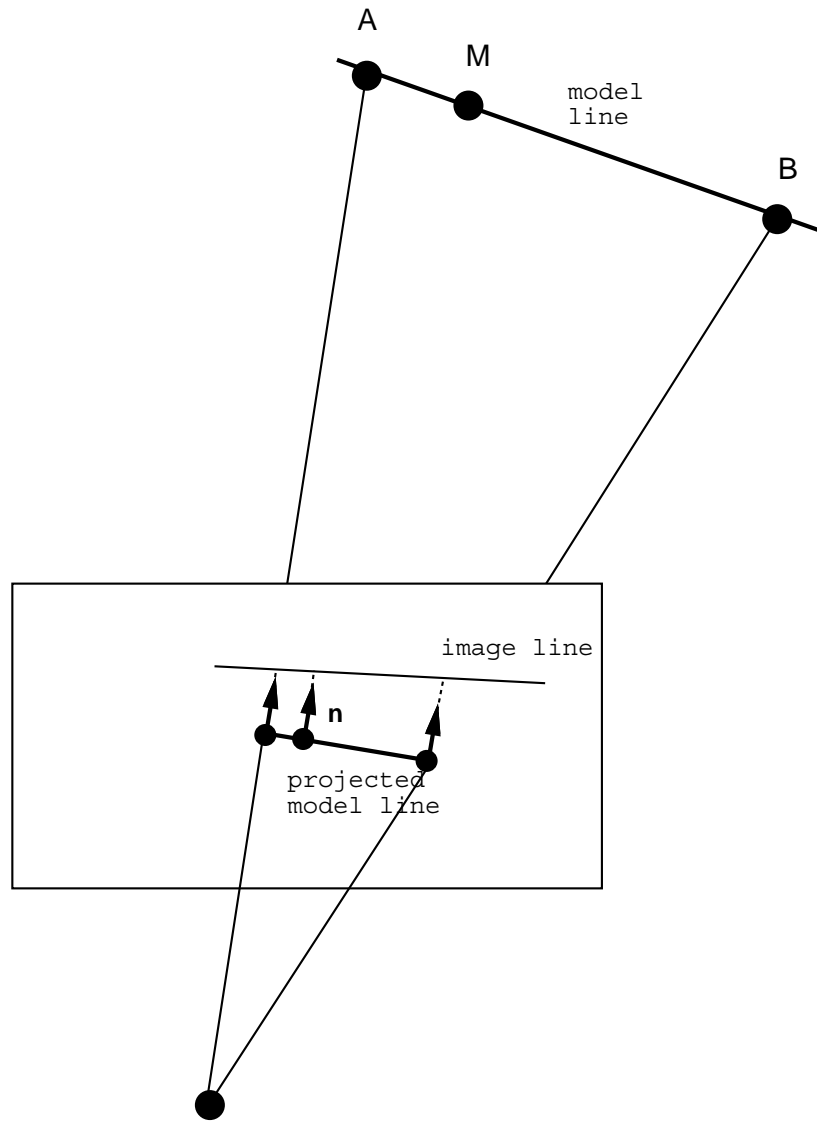


Figure 2: This figure shows a match between a model point (lying onto a straight-line and an image line, i.e., a point-to-line correspondence).

The Jacobian associated with this configuration – three colinear points matching an image contour – writes, i.e., eqs. (9), (13), and (10):

$$\mathbf{J}_2 = \frac{\mathbf{p}}{\|\mathbf{p}\|} \begin{bmatrix} \frac{1}{z_A^2} & 0 & 0 \\ 0 & \frac{1}{z_B^2} & 0 \\ 0 & 0 & \frac{1}{z_M^2} \end{bmatrix} \begin{bmatrix} -p_u z_A & -p_v z_A & p_u x_A + p_v y_A \\ -p_u z_B & -p_v z_B & p_u x_B + p_v y_B \\ -p_u z_M & -p_v z_M & p_u x_M + p_v y_M \end{bmatrix} \quad (16)$$

$$\left[\begin{array}{l} p_u x_A y_A + p_v (z_A^2 + y_A^2) \quad -p_u (z_A^2 + x_A^2) - p_v x_A y_A \quad p_u y_A z_A - p_v x_A z_A \\ p_u x_B y_B + p_v (z_B^2 + y_B^2) \quad -p_u (z_B^2 + x_B^2) - p_v x_B y_B \quad p_u y_B z_B - p_v x_B z_B \\ p_u x_M y_M + p_v (z_M^2 + y_M^2) \quad -p_u (z_M^2 + x_M^2) - p_v x_M y_M \quad p_u y_M z_M - p_v x_M z_M \end{array} \right]$$

By substituting the coordinates of \mathbf{M} and \mathbf{p} with their expressions as functions of the coordinates of \mathbf{A} and \mathbf{B} we obtain that the third row of the 3×6 matrix above is a linear combination of the first and second rows. Therefore the rank of \mathbf{J}_2 is equal to 2. In other terms, points M_i which are collinear with A and B are redundant. Regardless of the number of points the rank of the Jacobian associated with n collinear points matching an image line is at most equal to 2.

4.2 Varying focal length

The Jacobian is a 3×7 matrix in this case. The first six columns are identical to eq. (16). The last column is obtained by combining the expression of matrix \mathbf{N} with eq. (14) and is equal to:

$$\begin{aligned} & \frac{z_A}{f} (p_u x_A + p_v y_A) \\ & \frac{z_B}{f} (p_u x_B + p_v y_B) \\ & \frac{z_M}{f} (p_u x_M + p_v y_M) \end{aligned}$$

As before, by substitution, we obtain the third row as a linear combination of the first two. Therefore the rank of the 3×7 Jacobian matrix is equal to 2.

4.3 Varying internal camera parameters

The Jacobian is a 3×9 matrix in this case. The first seven columns are identical to the previous case. The last two columns are obtained by combining the expression of matrix \mathbf{N} with eq. (15) and yield the following 3×2 block:

$$\begin{array}{cc} \frac{z_A^2 p_u}{f} & \frac{z_A^2 p_v}{f} \\ \frac{z_B^2 p_u}{f} & \frac{z_B^2 p_v}{f} \\ \frac{z_M^2 p_u}{f} & \frac{z_M^2 p_v}{f} \end{array}$$

Again, the rank of this matrix is equal to 2.

5 Multiple camera tracking

Single-camera tracking suffers from three basic limitations:

- As explained above, there are cases where the Jacobian matrix is rank-deficient and hence tracking cannot be performed (planar objects lying in a fronto-parallel plane);
- Due to occlusions, bad imaging conditions, and so forth, there may not be enough features available in one image, and
- While the object moves it may, totally or partially, disappear from the camera field of view.

There are two options enabling one to introduce multiple-camera tracking. The first possibility is to make use of multiple-camera geometry, as described in several books [8], [10], [18], and which implies that all cameras have a large field of view in common. The second possibility is to execute single-camera trackers in parallel while making explicit the object's rigidity.

Indeed, if each one of the cameras looks at a different object part, the whole object is nevertheless rigid and geometric knowledge allows individual calibration of each one of the cameras. Once this calibration step has been performed, all the cameras track the object in parallel estimating its motion in a common reference frame. Such a tracker allows, one feature to be seen by one camera, another feature to be seen by another camera, etc.

Since the latter method does not use any form of stereo correspondence, the cameras can be quite far apart thus insuring that a planar piece of the object appearing in one's camera fronto-parallel plane is viewed slanted by the other cameras. Moreover, even if each camera sees planar features in its own fronto-parallel plane, the Jacobian matrix resulting from all cameras is not rank deficient.

5.1 The multiple camera Jacobian matrix

Without loss of generality, we consider that each camera has been individually calibrated using the tracker described in the previous section in conjunction with a static object. This means that both internal and external (pose) parameters are available for each camera and that the position and orientation of each camera is known in a common reference frame.

Therefore the multiple camera tracker is left with six parameters to be estimated: the position and orientation of the object with respect to the common reference frame.

With the same notations as above, we generalize the point-to-point Jacobian matrix such that the reference frame is an arbitrary frame rather than the camera frame. For camera k the Jacobian writes:

$$\mathbf{J}_1^k = \begin{bmatrix} \vdots \\ -\frac{1}{z_{ik}} & 0 & \frac{x_{ik}}{z_{ik}^2} & \frac{x_{ik}y_{ik}}{z_{ik}^2} & -\left(1 + \frac{x_{ik}^2}{z_{ik}^2}\right) & \frac{y_{ik}}{z_{ik}} \\ 0 & -\frac{1}{z_{ik}} & \frac{y_{ik}}{z_{ik}^2} & \left(1 + \frac{y_{ik}^2}{z_{ik}^2}\right) & -\frac{x_{ik}y_{ik}}{z_{ik}^2} & \frac{-x_{ik}}{z_{ik}} \\ \vdots \end{bmatrix} \begin{bmatrix} \mathbf{R}_k & [\mathbf{t}_k]_{\times} \mathbf{R}_k \\ 0 & \mathbf{R}_k \end{bmatrix} \quad (17)$$

where \mathbf{R}_k and \mathbf{t}_k are the rotation and translation mapping 3-D coordinates of model points from a global common reference frame to the camera frame. The notation $[\]_{\times}$ stands for the skew symmetric matrix associated with a 3-vector, x_{ik} , y_{ik} , and z_{ik} represent the coordinates of a model point i in camera frame k .

The multiple camera Jacobian matrix writes:

$$\mathbf{J}_1 = \begin{bmatrix} \mathbf{J}_1^1 \\ \vdots \\ \mathbf{J}_1^k \\ \vdots \end{bmatrix} \quad (18)$$

There is a similar expression for the point-to-contour multiple-camera Jacobian matrix:

$$\mathbf{J}_2 = \begin{bmatrix} \mathbf{N}^1 \mathbf{J}_1^1 \\ \vdots \\ \mathbf{N}^k \mathbf{J}_1^k \\ \vdots \end{bmatrix} \quad (19)$$

To conclude, with two or more cameras the tracker is well conditioned. Such configurations as cameras with parallel image planes may cause problems ($\mathbf{R}_k = \mathbf{I}$ in eq. (17)) but such configurations can easily be avoided. Moreover, they are not of very useful in practice.

6 Experiments

The single and multiple camera tracking methods described above were used to locate complex ship parts for subsequent ship building operations such as welding [14].

Throughout the experiments we used two RGB frame grabbers in conjunction with 6 black-and-white cameras. This hardware setup guarantees image grabbing synchronization. The cameras are thus interfaced to a PC/Pentium3 (733MHz) running under Linux. The image size is 768×574 pixels. The tracker runs at 25Hz with one camera, at 17Hz with two cameras, at 12Hz with three cameras, ... and at 6Hz with six cameras. This corresponds to the object model described below which is relatively complex.

We found that the most practical configurations use 2 to 4 cameras. These computation speeds correspond to one iteration of a tracker per image. Performing several iterations per image has theoretical advantages in the sense that convergence of the tracker is guaranteed. However, it is undesirable in practice because it degrades the speed and therefore it limits the system to slow moving objects.

The object to be located is modeled with both straight and curvilinear edges. There are approximatively 300 model edges. Both these edges (straight and curvilinear) are approximated by piecewise polygonal lines formed of short segments: Each edge is sampled such that, on an average there are 10 points per model edge.

6.1 Finding point-to-contour correspondences

One of the most crucial steps of any tracking method is to establish matches (or correspondences). In our case we must associate model edges with image contour points. Such associations are easier to find than the classical point-to-point, line-to-line, or contour-to-contour matches. The method described below is noise-, error-, and occlusion-tolerant because it eliminates any model-to-image data associations that are likely to lead to an ambiguous solution.

The first step in the model-to-image data association method is to predict model edges that are visible in the image. Using the current pose of the model with respect to one camera, a z-buffer is produced from the object model (represented under the VRML 2.0 description format). Z-buffering has linear complexity in the number of model primitives. Each visible model-edge has a color index associated with it while the hidden edges together with the model faces are coloured in black. Hence it is straightforward to determine whether a point belonging to a model edge is visible or not: It is sufficient to index its color. This model representation is illustrated on Figure 3.

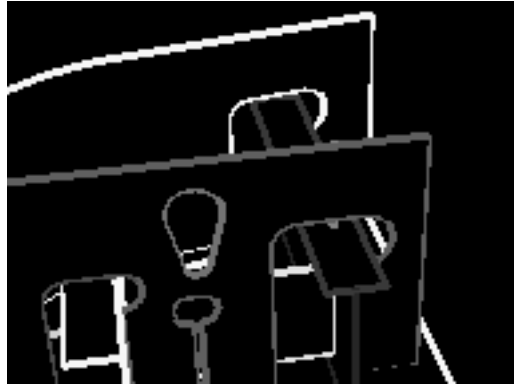


Figure 3: This figure shows a z-buffer associated with an image from a predicted point of view. Black indicates that there is no visible edge. Each visible edge is indexed with a different colour.

The second step is to search image contours in a direction perpendicular to the predicted model edge, on its both sides. In practice, one-dimensional edge detection is performed for each model point along a line perpendicular to its supporting model edge. This one dimensional search and edge detection is illustrated on Figures 4 and 5.

Figure 4 shows a model edge, points along this edge (black dots) and the image points that are eventually associated with each one of these points (grey dots). Two types of edge profiles are present in the data: step and roof edges. Steps correspond to classical intensity changes. Roofs correspond to the presence in the model of thin plates. It is not always possible to detect the contours on both sides of a thin plate. Therefore we decided to fuse these contours into a unique central one. A step edge is shown on Figure 5-left and a roof edge is shown on Figure 5-right.

The third step consists of associating an image edge-point with a model contour. This matching is done on the basis of the presence/absence of an edge along the direction of search within a “short distance” away from the predicted model contour. Figure 6 shows an example. A number of model

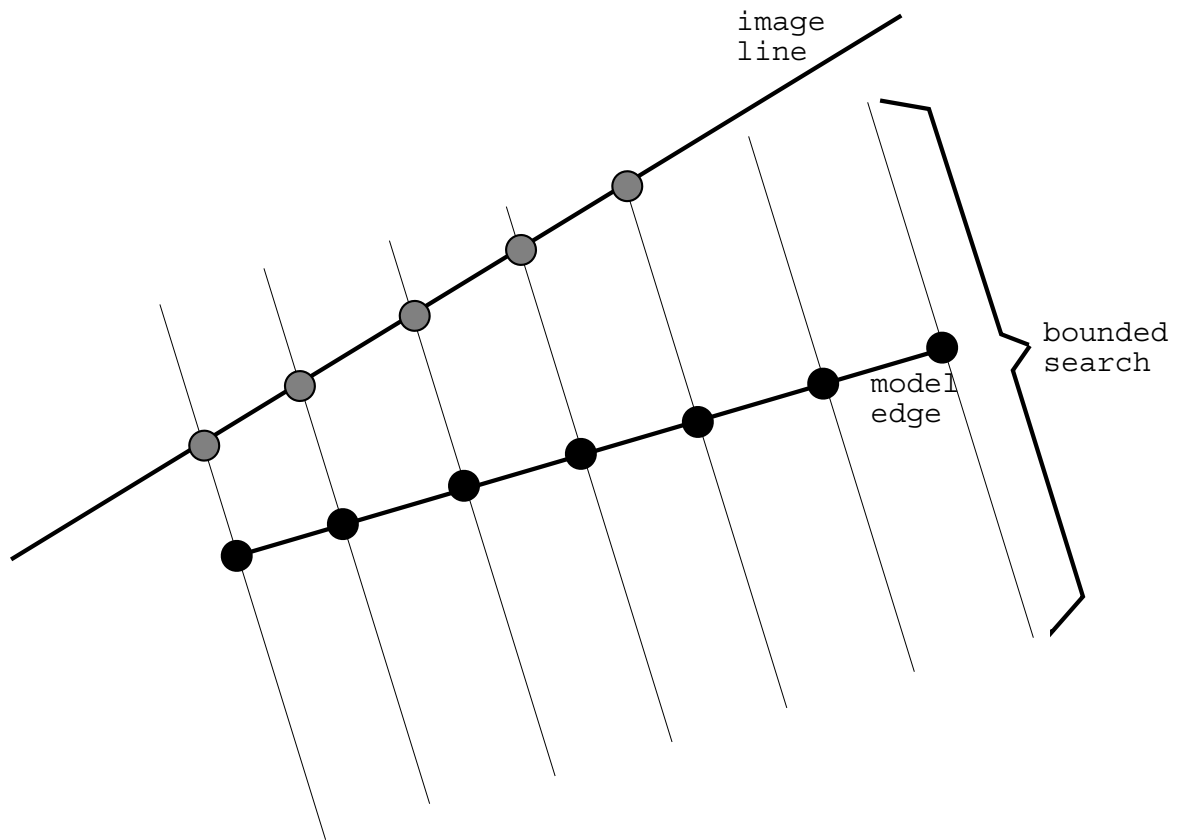


Figure 4: Point-to-contour (here point-to-line) correspondences are established by searching for image points around a predicted model point lying onto a model edge. The search is in a direction perpendicular to the predicted model edge and is bounded.

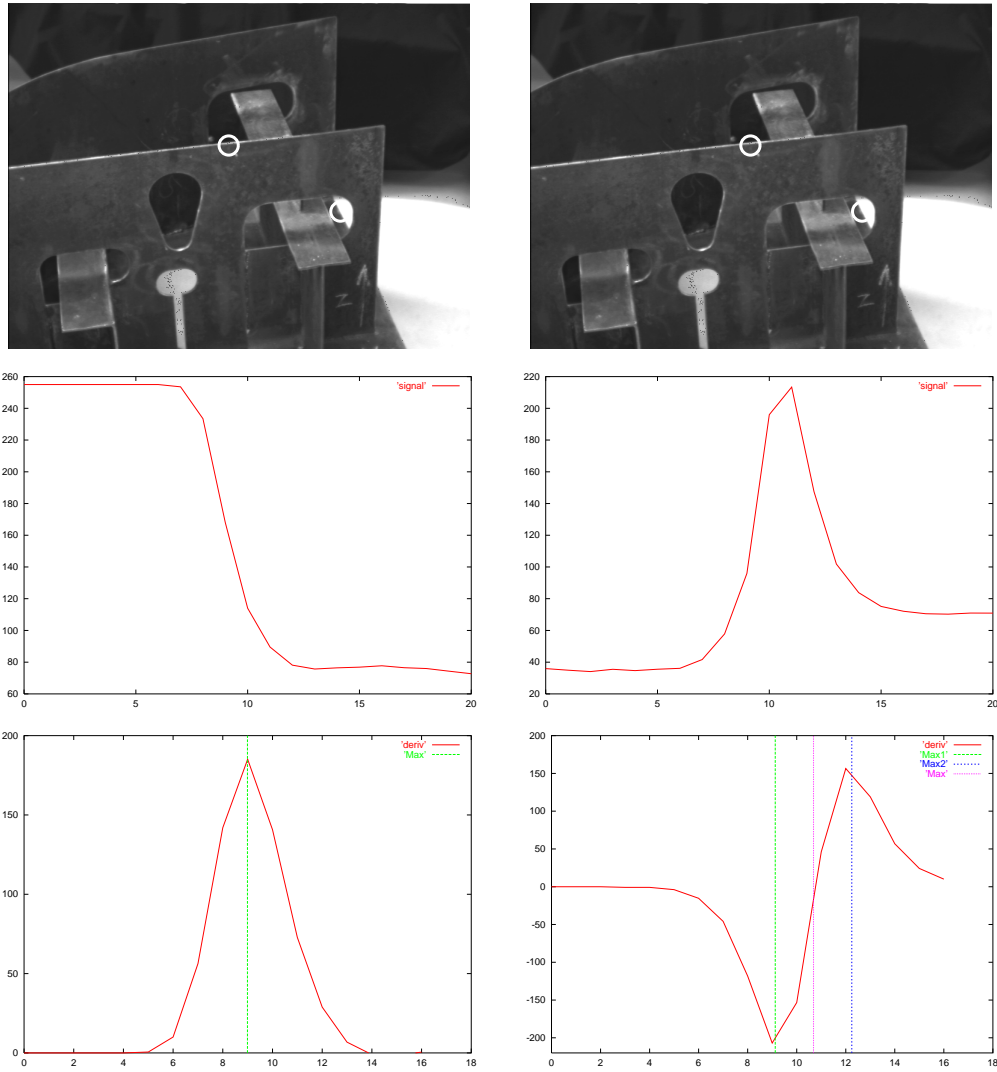


Figure 5: The data contains both step (left) and roof (right) edges. The former are classical intensity changes. The latter correspond to the presence of a thin plate. The intensity-profile derivative is first computed (middle) and local maxima are located (bottom). Whenever two local maxima are located and if their magnitudes are similar, then a roof edge is reported and the edge is located as a zero-crossing (bottom-right).

edges are predicted in the image. The small white segments show successful associations of model contours with image edge points. Notice that a large number of model contours do not have edge points associated with them either because of occlusions or because an image edge has not been found.

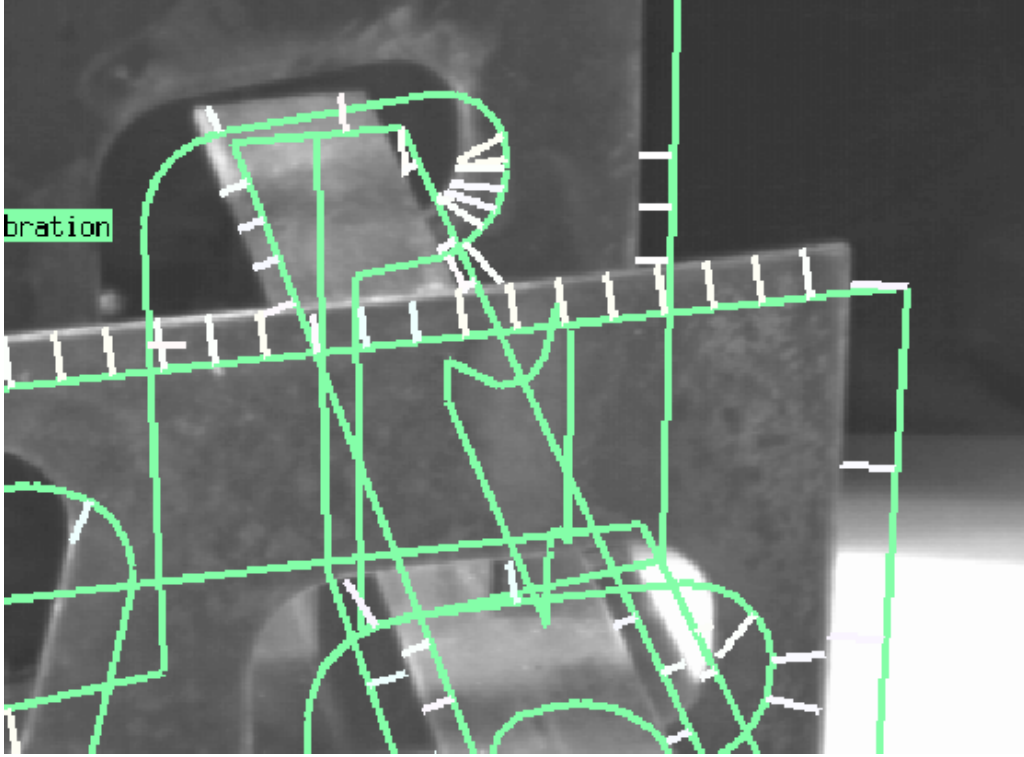


Figure 6: Points along model edges are associated with image points – these model-contour-to-image-point correspondences are illustrated by short segments perpendicular to the model edges. Notice that a large number of model edges do not have image points associated with them. The ability to restrict the number of matches to the most reliable ones is key to successful convergence of the tracking process.

6.2 Locating a static object

The first experiment consists of using one camera with fixed internal parameters observing a static object. A complete object location sequence is shown on Figure 7. The initial model location was set manually. After 18 iterations the pose parameters converged to a stable solution corresponding to an average image error of 0.8 pixels.

Each iteration comprises (i) the gathering of a new image, (ii) model prediction in the image using the previously estimated pose parameters,

(iii) hidden-line elimination, (iv) detecting an image contour match for each model point, and (v) one Gauss-Newton iteration based on valid point-to-contour correspondences. Since with one camera the algorithm runs and 25Hz, it takes 0.7 seconds to reach convergence in this case.

Once convergence is reached, the system is ready for tracking.

6.3 Tracking the focal length

The second experiment consists of using one camera with varying focal length observing a static object. The focal length varies back and forth from its minimal to its maximal values with a ratio of 1:3. The left column of Figure 8 shows the result of tracking in such a case. Both the pose and the focal length are allowed to vary during the tracking process using the adequate Jacobian matrix, i.e., sections 3.2 and 4.2.

The right column of Figure 8 shows the same experimental setup but the focal length is set to a fixed value. The tracker tries to compensate the zoom effect with depth variations but, clearly, the results are not very good.

Table 1 summarizes a series of tests. The first test (top) is designed to track the focal length as just described. Small variations in depth are due to the fact that the optical center moves while the zoom varies. The second test (middle) maintains the focal length to its initial value and therefore the depth compensates for zoom variations. The third test (bottom) allows both internal and external parameters to vary. Although the optical center moves a lot, the focal length values estimated in this case are very close to those estimated in the first test.

This is clear experimental evidence that the method described in this paper is able to make a clear distinction between depth variations and zoom variations. The only case that confuses the tracker is when the object is planar and lies in a fronto-parallel plane.

6.4 Camera calibration during tracking

Modern digital cameras have built-in auto-focus. The ability to track an object with such a camera necessitates on-line estimation of internal camera parameters because a change in focus is associated with changes in internal camera parameters.

The third experiment consists of estimating the internal camera parameters – tracking with one camera and 9 parameters while the object is allowed to move. Starting with a good initial guess and after only a few iterations,

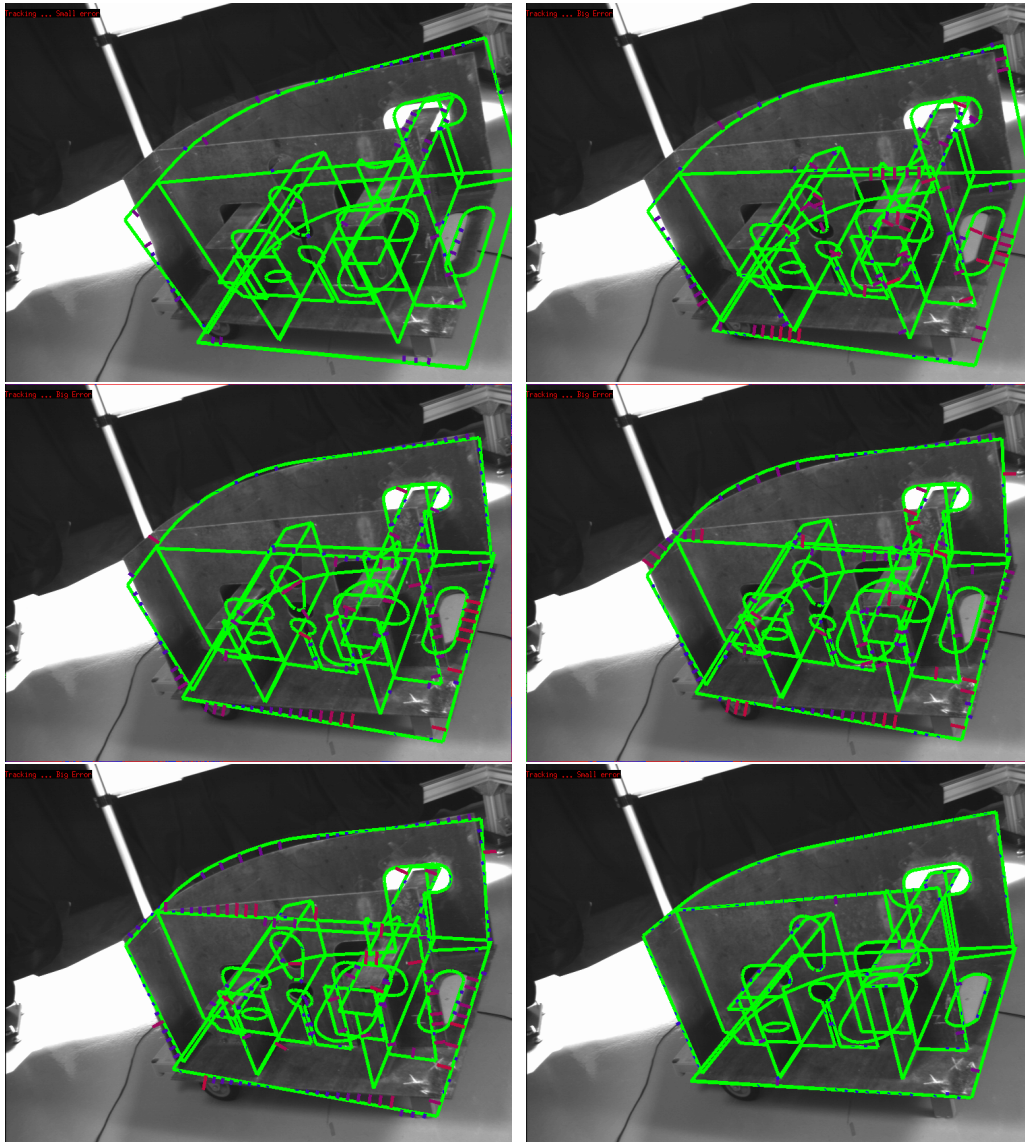


Figure 7: This figure shows an object location example from initialization to convergence. 18 iterations were necessary in this case. The figure shows (left to right and top to down) the initialization, as well as iterations 3, 6, 9, 12, and 18. Although the algorithm performs hidden-line elimination and considers only the model points predicted visible, the on-line display shows all (visible and hidden) model edges.

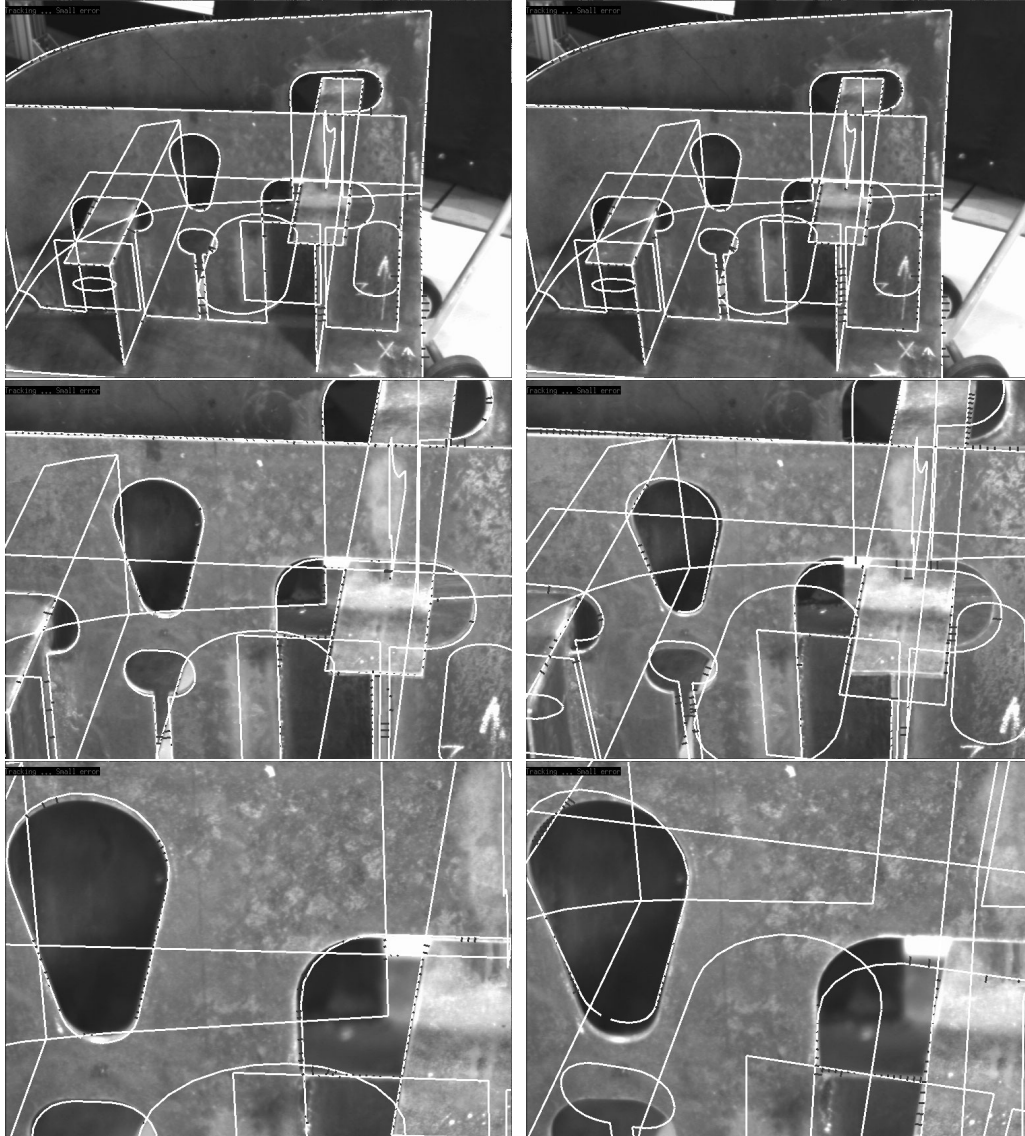


Figure 8: The effect of zooming in and zooming out can be taken into account by the tracker (left column). The right column shows the effect of tracking with fixed focal length: the zoom effect is compensated by variations in depth, but this compensation is far from being perfect.

	f (pixels)	u_0 (pixels)	v_0 (pixels)	Depth (mm)
Focal length &	1615.2	288.4	386.8	2351.7
External	3226.4	288.4	386.8	2503.7
Parameters	4899.5	288.4	386.8	2553.4
External	1569.8	289.0	386.3	2282.1
Parameters	1569.8	289.0	386.3	1293.8
	1569.8	289.0	386.3	840.2
All	1566.7	288.4	386.8	2476.8
Parameters	3190.2	335.5	623.7	2512.3
	4956.2	164.4	105.2	2527.5

Table 1: This table shows a series of three tests where only the focal length varies in practice.

the tracker converges such that the estimated camera parameters match the real values.

In order to assess the quality of the estimated camera parameters we compared the results of tracking with the result obtained by using a calibration jig, Table 2. The first row displays parameter values determined off-line using a classical camera calibration technique in conjunction with a calibrated object (the accuracy of the 3-D measurements are of about 0.01mm). The subsequent rows correspond to experiments performed with the tracker. Each experiment consists of 100 measurements. Each experiment correspond to a different setup – a different relative position between object and camera.

The discrepancies between the two sets of parameters appear from the fact that the ship part is a welded object which does not perfectly correspond to its CAD model. The accuracy of the ship part real size with respect to its theoretical CAD representation is of the order of a few millimeters.

6.5 Tracking with three cameras

The last experiment that we describe uses 3 static cameras observing a moving object. With three cameras the tracking system runs at 12Hz thus allowing objects to freely move in the viewing volume. Notice that the camera setup is arbitrary, no common field of view in between any camera pair is necessary. One camera has a panoramic field of view while the other two cameras zoom onto various object parts.

The camera system is calibrated using the previously described experiments for each individual camera. During this experiment the internal camera parameters associated with all three cameras are fixed as well as the

	f_u	std	u_0	std	v_0	std
off-line	1524.5		283.1		400.2	
Exp. 1	1468.7	3.1	282.8	1.6	376.6	1.2
Exp. 2	1479.6	4.2	321.7	2.2	349.1	3.2
Exp. 3	1490.1	2.65	317.2	2.1	347.9	2.6
Exp. 4	1458.4	3.1	263.2	1.4	366.1	1.6
Exp. 5	1433.3	3.24	254.1	3.91	380.5	1.94
Exp. 6	1554.3	0.83	286.0	1.50	338.9	0.76

Table 2: The internal camera parameters obtained with classical off-line calibration (first row) are compared with those obtained during the tracking process.

relative positions and orientations of the cameras. Therefore the Jacobian used by the tracker is given by eq. 19. From the Jacobian singularity analysis carried out above it is clear that such a 3 camera tracker has no singularity associated with it. The minimal data association required by the tracker is composed of 6 model points matching 3 image contours, with two points matching one contour.

In practice, the tracker has to deal with partial occlusions in all images, global occlusion in one or two images, deficiency of one or two cameras, etc. The advantage of the 3 camera system is that the minimal matching requirement just described may be distributed. The tracker is able perform well with as little matches as two colinear model points visible in each one of the 3 images.

The next three figures show the result of tracking with three cameras. Figure 9 shows a typical tracking sequence where the object freely moves onto the ground. Notice the excellent overlapping between model and object through the whole sequence in spite of the fact that the object travels away from the field of view of two cameras. Figure 10 shows partial occlusion in two images and total occlusion in one image while Figure 11 shows partial occlusion in all three images.

7 Discussion

In this paper we described a method for tracking rigid objects using one or several cameras. The tracking process consists of aligning a 3-D model representation of an object with images by measuring and minimizing the image error between predicted model contours and image edge points. The tracker

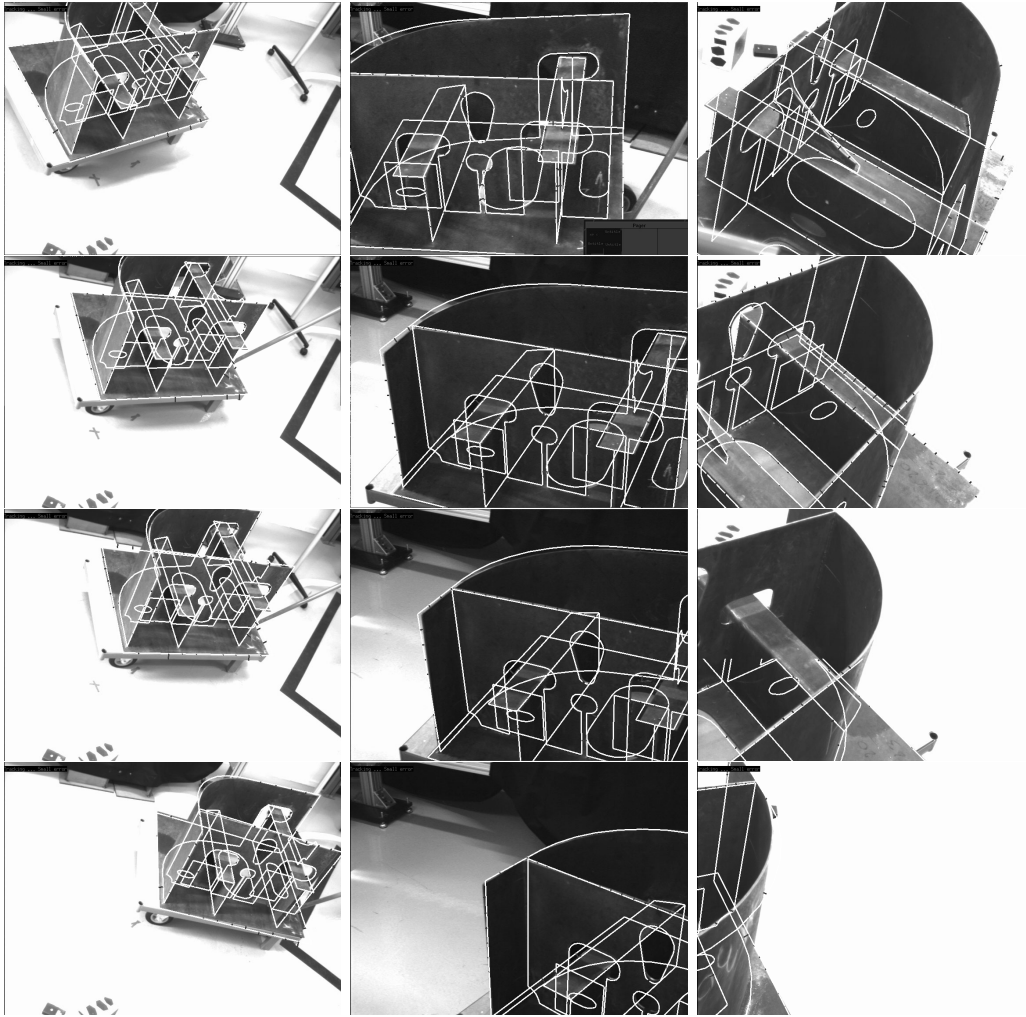


Figure 9: A tracking sequence. The object rotates and translates onto the floor. Notice that the three cameras have very different points of view.

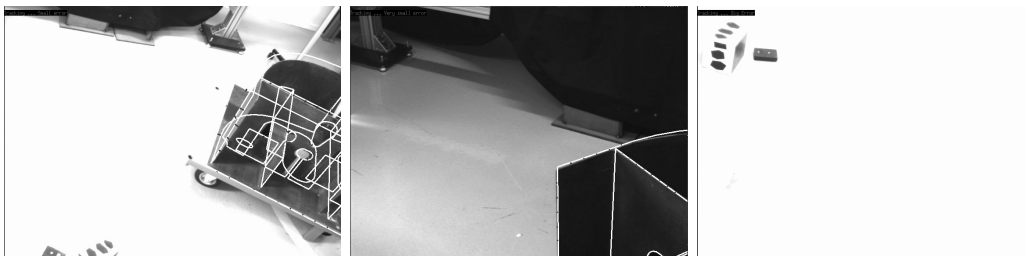


Figure 10: Total occlusion in one image and partial occlusion in two images.

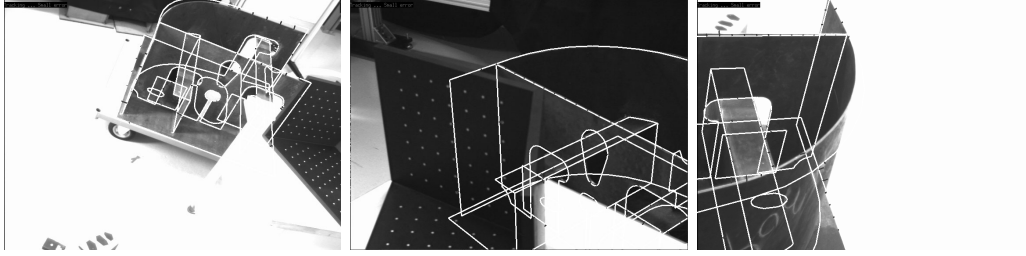


Figure 11: Partial occlusion in three images.

behaves like a visual servo loop where the internal and external camera parameters are updated at each new image acquisition.

We studied in detail the Jacobian matrix associated with this minimization process in the presence of both point-to-point and point-to-contour matches. We established the minimal number of matches that are needed as well as the singular configurations leading to a rank-deficient Jacobian matrix. We established a mathematical link between the point-to-point and point-to-contour cases. Based on this link we showed that the latter has the same kind of singularities than the former. Moreover, we studied multiple camera configurations which optimize the robustness of the method in the presence of single-camera singularities, bad, noisy, or missing data.

Extensive experiments done with a complex ship part and with up to three cameras validated the method. In particular we show that the tracker may well be used as a camera calibration procedure.

One limitation of the method is that it only deals with edges. In complex natural and industrial environments an edge-based method has failures. Therefore we plan to incorporate texture information with our model representation. When a model edge is predicted in the image, nearby model texture is predicted as well and hence it is possible to measure the discrepancy with image texture and tune the tracked parameters by optimizing the alignment between model and image textures.

The fusion of several cues such as edge and texture information, combined with the increasing computing power available today, is likely to improve the robustness and reliability of visual trackers for many robotics applications.

References

- [1] M. Armstrong and A. Zisserman. Robust object tracking. In *Proc. Asian Conference on Computer Vision*, volume I, pages 58–61, 1995.

- [2] Q. Delamarre and O. Faugeras. 3D articulated models and multi-view tracking with silhouettes. In *Proceedings 7th IEEE International Conference on Computer Vision*, volume 2, pages 716–721, Corfou, Greece, September 1999.
- [3] T. Drummond and R. Cipolla. Real-time tracking of complex structures for visual servoing. In *Proc. IEEE Seventh Int. Conf. on Computer Vision, Corfu, Greece, 20-25 September, 1999*.
- [4] T. Drummond and R. Cipolla. Real-time tracking of complex structures for visual servoing. In *Vision Algorithms, Theory and Practice*, pages 69–83. Springer Verlag, LNCS, 1999.
- [5] T. Drummond and R. Cipolla. Real-time tracking of complex structures with on-line camera calibration. In *Proceedings of British Machine Vision Conference*, volume 2, pages 574–583, Nottingham, UK, September 1999.
- [6] T. Drummond and R. Cipolla. Real-time tracking of multiple articulated structures in multiple views. In *Proceedings of 6th European Conference on Computer Vision*, volume 2, pages 20–36, Dublin, Ireland, June-July 2000.
- [7] B. Espiau. Effect of camera calibration errors on visual servoing in robotics. In *Proceedings of the Third International Symposium on Experimental Robotics*, pages 187–193, Kyoto, Japan, October 1993.
- [8] O. D. Faugeras. *Three Dimensional Computer Vision: A Geometric Viewpoint*. MIT Press, Boston, 1993.
- [9] C. Harris and Stennett C. RAPID – A video rate object tracker. In *Proceedings of the First British Machine Vision Conference*, pages 73–78, Oxford, September 1990.
- [10] R. Hartley and A. Zisserman. *Multiple View Geometry in Computer Vision*. Cambridge University Press, Cambridge, UK, 2000.
- [11] R. Horaud, G. Csurka, and D. Demirdjian. Stereo calibration from rigid motions. *IEEE Transactions on Pattern Analysis and Machine Intelligence*, 22(12):1446–1452, December 2000.
- [12] S. Hutchinson, G. D. Hager, and P. I. Corke. A tutorial on visual servo control. *IEEE Transactions on Robotics and Automation*, 12(5):651–670, October 1996.

- [13] K. Kinoshita and K. Deguchi. Simultaneous determination of camera pose and intrinsic parameters by visual servoing. In *Proceedings of the 12th IAPR International Conference on Pattern Recognition*, volume 1, pages 285–289, Jerusalem, September 1994.
- [14] B. Lamiroy, T. Drummond, R. Horaud, and O. Knudsen-Neckelman. Visually guided robots for ship building. In *1st International Conference on Computer Applications and Information Technology in the Maritime Industries (COMPIT'2000), Potsdam/Berlin, Germany, March 30 – April 2, 2000*.
- [15] B. Lamiroy, B. Espiau, N. Andreff, and R. Horaud. Controlling robots with two cameras: How to do it properly. In *Proc. of IEEE International Conference on Robotics and Automation*, pages 2100–2105, San Francisco, CA, April 2000.
- [16] D. Lowe. Fitting parameterized three-dimensional models to images. *IEEE Transactions on Pattern Analysis and Machine Intelligence*, 13(5):441–450, May 1991.
- [17] D. Lowe. Robust model-based motion tracking through the integration of search and estimation. *International Journal of Computer Vision*, 8(2):113–122, 1992.
- [18] Q.-T. Luong and O. D. Faugeras. *The Geometry of Multiple Images*. MIT Press, Boston, 2001.
- [19] E. Marchand, P. Bouthemy, F. Chaumette, and V. Moreau. Robust real-time visual tracking using a 2D-3D model-based approach. In *Proceedings 7th IEEE International Conference on Computer Vision*, volume 1, pages 262–268, Corfou, Greece, September 1999.
- [20] T. Q. Phong, R. Horaud, A. Yassine, and D. T. Pham. Object pose from 2-D to 3-D point and line correspondences. *International Journal of Computer Vision*, 15(3):225–243, July 1995.
- [21] C. Rasmussen and G. D. Hager. Probabilistic data association methods for tracking complex visual objects. *IEEE Transactions on Pattern Analysis and Machine Intelligence*, 23(6):560–576, June 2001.
- [22] R.L. Thompos, I.D. Reid, L.A. Munoz, and D.W. Murray. Providing synthetic views for teleoperation using visual pose tracking in multiple caeras. *IEEE Transactions on Systems, Man, and Cybernetics–Part A: Systems and Humans*, 1(31):43–53, January 2001.

- [23] M. Tonko and H-H. Nagel. Model-based stereo-tracking of non-polyhedral objects for automatic disassembly experiments. *International Journal of Computer Vision*, 37(1):99–118, June 2000.
- [24] M. Vincze, M. Ayromlou, W. Ponweisser, and M. Zillich. Edge-projected integration of image and model cues for robust model-based object tracking. *International Journal of Robotics Research*, 20(7):533–552, July 2001.